

Design and scaling of an Omega-EP experiment to study cold streams feeding early galaxies

SHANE X. COFFING,^{1,2} ADRIANA A. ANGULO,¹ MATTHEW R. TRANTHAM,¹ YUVAL BIRNBOIM,³ CAROLYN C. KURANZ,¹
R.P. DRAKE,¹ AND GUY MALAMUD^{1,4}

¹*Center for Laser Experimental Astrophysical Research, University of Michigan, Ann Arbor, USA*

²*Computer, Computational and Statistical Sciences (CCS) Division, Los Alamos National Laboratory, New Mexico, USA*

³*Racah Institute of Physics, The Hebrew University, Jerusalem, Israel*

⁴*Department of Physics, Nuclear Research Center e Negev, Beer-Sheva 84190, Israel*

ABSTRACT

Galaxies form in the centers of dark matter halos, and grow by accreting gas from the halos. The gas supply to the galaxy is the bottleneck for star formation and ultimately sets its stellar mass and star formation rate. As gas falls from the cosmic web into the halos, the highly supersonic infalling gas (Mach ~ 20 for Milky Way typed halos) eventually forms a shock. If cooling is inefficient, this shock quickly stabilizes as a quasi-static, slow expanding, accretion shock at the outer edge of the halo. If, however, cooling is important, a recent theory suggests that filaments of gas from the cosmic web will free-fall through the halos unshocked, and shock only at the outskirts of the central galaxies. These ‘cold streams’ allow for a steady supply of gas into the galaxies, and more efficient star formation. The cold, dense filament flowing into a hot, less dense environment is potentially Kelvin-Helmholtz unstable. This instability may hinder the ability of the stream to deliver gas deeply enough into the halo. A design of a well-scaled laser experiment on Omega EP meant for studying this phenomena is presented in the current work, with relevant theory informed by 2D hydrodynamic simulations of the experiment. We establish the hydrodynamic scaling analysis between the cosmological system and its experimental analogue, presenting the experiment as an adiabatic upper limit to informing the role of mixing due to the KH instability.

Keywords: Kelvin-Helmholtz instability — galaxy formation — shock wave — halos

1. INTRODUCTION

The star formation rate in galaxies, that sets their mass and color, is regulated by the availability of gas within the galaxy. The amount of gas within the galaxy depends on the accretion rate for gas from the halos that surround them. Therefore, the hydrodynamic and thermodynamic conditions in the halos, and the rate at which gas is channelled into galaxies, is key to understanding galaxy formation and evolution. The idealized picture of galaxy formation is that gas and dark matter spherically condense due to their own self gravity, and eventually establish a dark matter halo and a gaseous halo. For the gas, an accretion shock thermalizes the

infalling gas. Behind the shock, the gas is almost hydrostatic, having converted its gravitational energy into kinetic, and finally into thermal energy at the shock. According to the virial theorem, the thermal component should roughly equal (up to a minus sign) half of the gravitational potential energy (Silk 1977; Rees and Ostriker 1977; White and Rees 1978). For halos comparable to the Milky-way’s halo ($M_v \sim 10^{12} M_\odot$) the corresponding virial temperature is $T_v \sim 10^6$ K. This picture holds as long as the radiative cooling is inefficient. Then, a virial shock quickly extends to the edge (the “virial radius”) of the halo. This condition is satisfied as long as the compression rate of the gas below the virial shock is faster than the cooling rate, which requires that the halo mass be larger than a critical mass of $M_{shock} \sim 10^{12} M_\odot$ (Birnboim and Dekel (2003)). Gas infalling into halos below the critical mass is not expected to shock until it reaches the central galaxy. At low redshifts ($z \lesssim 1.5$, corresponding to around 9

Corresponding author: Shane X. Coffing
sxc@lanl.gov

Corresponding author: Guy Malamud
gmalamud@umich.edu

Gyrs ago) the transition around this critical mass is abrupt. This theoretical prediction is key to explain observed trends in low redshifts galaxies, particularly the bi-modality and sharp transition between smaller, blue (ie star-forming) galaxies, and larger red (non-star forming) galaxies (Baldry et al. 2004; Cattaneo et al. 2006). When a hot halo forms, additional feedback processes, particularly active galactic nuclei (AGNs) from the supermassive black holes at the centers of galaxies, can further halt gas accretion onto galaxies.

However, theory of the cosmic web (Zel'dovich 1970) and large, N-body cosmological simulations (Kereš et al. 2005; Springel et al. 2005; Dekel et al. 2009) imply that at higher redshifts ($z \gtrsim 1.5$), the infall onto halos around the critical mass scale is increasingly non-spherical, with the majority of the gas fed through narrow filaments that form the cosmic web. **Some recent observations argue that such cold streams have been observed (Bouché et al. 2016; Martin et al. 2019).** Since the cooling rate scales as the density squared, a mixed state, for which gas in the filaments free-falls inwards while the gas in-between filaments shocks and stops at the virial radius, occurs (Dekel and Birnboim 2006). This corresponds to cold filaments, infalling supersonically through hot, hydrostatic and diffuse medium. For masses just above the critical mass, these cold, dense streams are able to penetrate the hot circumgalactic medium (CGM) and deliver cold gas deep inside the halo, where it can be used to fuel galactic growth and form stars (Dekel and Birnboim 2006; Dekel et al. 2009). At redshift $z \gtrsim 2$ these filaments are on order of 1–10% of the virial radius $R_v \sim 100$ kpc in width, and are several orders of magnitude colder and denser than the CGM, reaching a temperature of $T_s \gtrsim 10^4$ K and density $\rho_s \sim 10 - 100\rho_b$, where subscripts s and b denote the filament/stream and background, respectively. These filaments are potentially able to resist the formation of a virial shock inside the filament due to much faster cooling rates (Birnboim et al. 2016). Without such a shock they may stay cold and collimated, providing substantial mass flow rates necessary for high star formation rates (Dekel et al. 2009).

Simulations resolving cold streams are only able to capture the large-scale structures and properties of the halo and filaments, such as radii, mean densities, and flow velocities. At finite resolutions of 100 pc, such as those of (Goerdt and Ceverino 2015), these simulations are unable to capture any small-scale features including the hydrodynamics at the boundary of the filament, the precise nature of a galactic boundary, and may not

preclude the coexistence of a shock somewhere near or inside the virial radius. Particularly unclear is the nature of a possible late shock emerging around $z \gtrsim 2$ in halos transitioning to above the critical mass. Some grid based codes observe fragmentation of the stream around $\sim 0.3R_v$ (Kereš and Hernquist 2009; Ceverino et al. 2010; Danovich et al. 2015). Springel et al. 2010 and Vogelsberger et al. 2012 found that filaments heat to roughly the virial temperature around $\sim 0.25-0.5R_v$. Additionally, modern Smooth-Particle-Hydrodynamics (SPH) codes that produce the bulk of galaxy formation studies tend to smooth out such accretion related shocks. Nelson et al. (2013) argued that SPH codes showing that streams remain cold and coherent were largely caused by numerical error inherent to SPH.

Some simulations show these streams maintain constant velocity from well outside the virial radius to deep within the halo, despite gravitational free-fall (Dekel et al. 2009). This suggests there is a dissipative process to shed off energy through the gain in gravitation potential. Despite possible means of emission that reveal loss of gravitational energy, the exact process is unclear, but may be in part due to hydrodynamic instability forming from large shear velocities at the filament edge. With the context of a cold, dense column of gas flowing through a hot, diffuse background, this shear flow may be subject to the Kelvin-Helmholtz instability (KHI), in which the velocity gradient across the interface of two fluids develops into vortical structures that greatly enhance mixing between the fluids.

Until recently (Mandelker et al. 2016; Padnos et al. 2018; Mandelker et al. 2019) the hydrodynamics of this cosmological process had not been considered in depth. In the study presented by Padnos et al. (2018), the KHI on the filament edge was considered in a simple numerical and analytical analysis, assuming no virial shock, and that the stream and background are in pressure equilibrium. They showed, that under relevant conditions, KHI might grow fast enough so the filament shape is dominantly controlled by its growth. **However, if the background pressure exceeds the material pressure inside the filament, a shock will be driven into the stream (Cornuault et al. 2018).** This shock has the potential to drastically alter the evolution of KHI, diminish the filament mass areal flux, and shut off cold matter deposition into the galaxy, potentially marking a possible transition between a cold stream embedded in hot media to purely hot mode accretion dominated by virial shock heating. **The lack in simulation capabilities to re-**

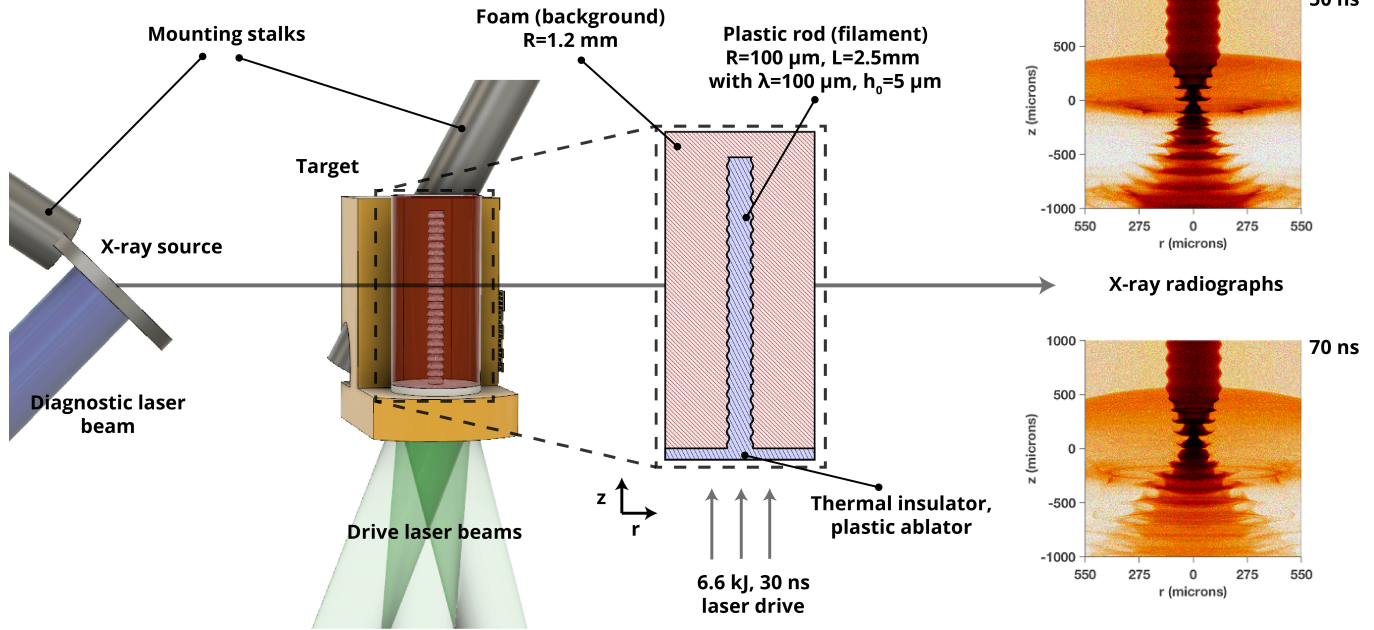


Figure 1. Current experimental design and sample simulated radiographs. From left to right in the figure, first the target is shown in Omega EP pointing geometry. Three laser beams deliver 6.6 kJ in 30 ns to the dense plastic of the cylindrical target, with a fourth beam driving a backlighter for x-ray radiography. The expanded view shows a cross-section of the part of the target in which the dynamics of interest occurs. On the far right are shown some sample radiographs at 50 and 70 ns into the experiment.

solve the small scale physics of these filamentary processes motivates our pursuit of a well scaled experiment, that might shed light on the matter. Furthermore, this platform experimentally provides an upper, idealized limit to the effect of the KHI, which can be scaled to the astrophysical case. We note that while asymmetry in the galaxy formation, filament orientation and shape, and virial shock are expected, we assume that the net structure of the shock is spherical and the filaments are columnar and oriented radially. Where the filament is expected to meet the shock at the virial radius, the shock is locally approximately planar and tangential to the infall direction of the filament. This provides a potential best-case scenario for KH growth. Finally, we note that small scale mixing on the filament edge, supposedly created due to energy transfer to small scales was not analyzed.

In this paper we present a preliminary design (shown in Fig. 1) of a high energy density laboratory experiment to emulate and study the cosmological process of a cold stream penetrating a shocked region within the galactic halo, collapse of the filament, and subsequent KHI evolution on the deflected interface of the shocked filament. **Our design builds upon previous work by**

(Malamud et al. 2013), which presented a way to study planar KHI in the compressible regime – the target presented here is essentially a cylindrical version of their Omega EP target utilizing a more powerful driven shock. The design of (Malamud et al. 2013) was motivated by earlier experiments to study shear flow under HED conditions using X-ray radiography (Hammel et al. 1994; Harding et al. 2009). The Omega laser facility has been successfully used to study the KH instability for a variety of configurations (Hurricane 2008; Harding et al. 2009; Hurricane et al. 2012; Smalyuk et al. 2013; Rutter et al. 2013), however this is the first that is capable of informing supersonic KHI on a cylindrical platform and is directly applicable to the study of cold streams. Section 2 discusses this platform along with the primary physics involved. We follow the work of (Mandelker et al. 2016; Padnos et al. 2018; Mandelker et al. 2019) to establish the parameter space for halos of $M \sim 10^{12} M_{\odot}$ around $z \sim 2$. We develop the physical description of the flow and present hydrodynamic simulations of the experiment using the CRASH radiation hydrocode (van der Holst et al. 2011). The scaling analysis necessary to determine a regime of applicability to the astrophysical process then follows. We identify an astrophysical regime in which KH significantly al-

ters the length where the filament converges about axis, thereby shock heating the cold filamentary material before it can reach the disk. This is highlighted in Section 3. We finally address the implications and limitations of our model, with discussion on the radiative regime and future work in Section 4.

2. EXPERIMENTAL DESIGN AND THE PHYSICS OF FILAMENT COLLAPSE

The primary assumption in our experimental design is that a columnar gaseous filament flows through the hot, shock-heated CGM and terminates in the galactic disk. High background pressures in the CGM are expected to exceed material pressure in the filament and thus drive a shock into the filament. We mimic this idealized process, using a cylindrical target designed for the Omega EP laser, wherein a laser driven shock causes a cylindrical plastic ‘filament’ (rod) to flow through a shock-heated foam ‘background’. The main diagnostic to be used in the experiment is X-ray radiography, which is capable of capturing an instance of this process, allowing a proper analysis of the rod edge. Fig. 1 shows the current experimental design and setup, in addition to sample simulated radiographs of the experiment.

In the following discussions, variables with the subscripts s and b will denote stream/filament (plastic rod experimental equivalent) and background (foam equivalent) quantities, respectively. Furthermore, when the two systems are discussed together, state variables with a superscript $*$ will be used for experimental quantities, where those without will be used for astrophysical quantities. The proposed target begins with a thin 50 μm plastic layer to which a 50 μm plastic thermal insulator and narrow rod assembly are attached. The rod assembly contains the physics package of the experimental platform. Single-wavelength $\lambda = 100 \mu\text{m}$ sinusoidal perturbations **of amplitude** $h_0 = 5 \mu\text{m}$ are machined on the plastic rod of diameter $d = 200 \mu\text{m}$ to seed the KH instability (KHI). This specific initial wavelength was chosen considering the experimental time and length scale, and is relevant to the scaling to the astrophysical system, discussed further below. A foam cylinder surrounds the plastic rod and is attached to the thermal insulator. The entire target is 2.6 mm in length and 1.2 mm in diameter.

The plastic layer, thermal insulator, and rod are identical in density (stream density $\rho_s = 1.4 \text{ g cm}^{-3}$) and polycarbonate material. The thermal insulator and rod contains a trace iodine dopant, but we consider all the plastics to be hydrodynamically equivalent. The dopant

is optically thick to x-rays: in the thermal insulator it serves to prevent unwanted radiative pre-heat from the laser pulse; in the rod it provides a sharp imaging contrast for x-ray radiography. The shell is a CH foam with a density of $\rho_b = 0.14 \text{ g cm}^{-3}$, placing our base density contrast at $\delta = \rho_s/\rho_b = 10$. This choice in contrast is again directly relevant to the ranges of density contrasts in the astrophysical case. Furthermore, a contrast of roughly 28 is accessible by dropping the foam density to $\sim 50 \text{ of mg cm}^{-3}$.

As mentioned, the experiment is designed for Omega-EP, which can provide up to a 30 ns long laser pulse delivering up to a total 6.6 kJ incident directly onto the plastic surface in a spot size of 1100 μm . Specifically for our design, Omega-EP will stitch three 351 nm wavelength, 10 ns pulses of 2.2 kJ each to assemble the primary laser drive and use the fourth beam for the x-ray radiography diagnostic. **The primary laser spot is spatially supergaussian (order 8), yielding an approximately flat-top shape.** The duration of the experiment is roughly $\tau_{exp} \sim 100 \text{ ns}$, and depending on the drive duration or energy delivered, diagnostics begin after $\sim 30 \text{ ns}$ of drive. Edge effects, such as inward propagating wall shocks caused by the unevenly heated plastic, are negligible as they arise on a timescale proportional to the foam thickness times the sound speed in the foam, **which is $\sim 2 - 10 \tau_{exp}$.** **Propagating wall shocks induced by this blow-off plastic plasma and other edge effects may be partially prevented or mitigated by using a beryllium shock tube casing, as will be considered in future experiments if needed.**

2.1. Deflection of the background-filament interface

Fig. 2 shows the density structure as predicted by a two-dimensional CRASH simulation in cylindrical, rz geometry at several times. CRASH is an Eulerian, radiation hydrodynamics code, designed to simulate laser experiments and high-energy density systems. **The long pulse laser is initialized at $t = 0 \text{ ns}$. The pulse drives a shock which proceeds from bottom to top, into the plastic.** After 1 ns, the shock progresses through the plastic layer. The shock continues to propagate through the plastic, crossing the thermal insulator interface at $t \sim 5 \text{ ns}$. By 20 ns, the shock has long exited the dense plastic, propagating through the physical package, while transmitting an oblique shock into the plastic rod. The filament collapses **inwards**, since the shock travels faster in the foam, compared to the rod. Note that the filament collapse converges cylindrically about axis. The shock reflects about the

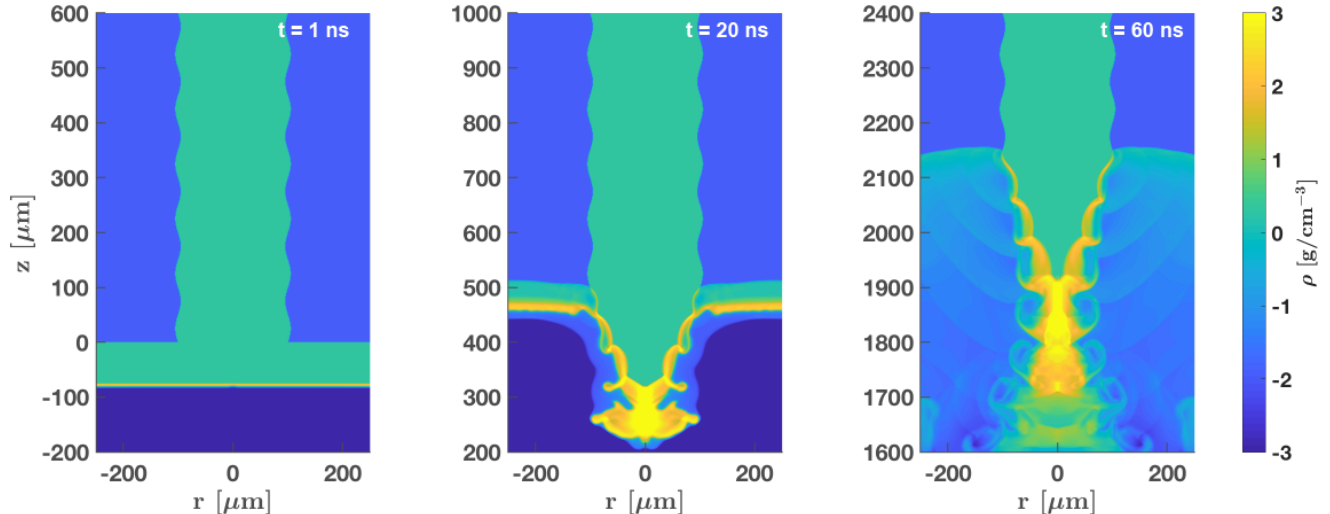


Figure 2. A pseudocolor plot showing the \log_{10} density of a CRASH simulation of the experimental system at three times during its evolution. (Left) The initial configuration at 1ns of laser drive. (Middle) 20ns into the drive, the filament has collapsed and begins to reflect axially. The incident and transmitted shocks are evident. (Right) The drive is in a desired configuration of the quasi-steady dynamics 30ns after the laser drive has ended (60 ns total). The shock reflections are visible in the foam due to interactions with the perturbed interface in addition to shock structure in the shocked filament. The apparent shock curvature is largely the consequence of laser energy deposition and not intended to replicate curvature in the astrophysical case.

axis, causing the filament to reflect cylindrically back outward into the shocked material downstream. The perturbations on the deflected foam-filament interface grow continuously throughout the collapse and reflection. This is well evident by 60 ns (right panel).

Two shocks are present: the incident, nearly planar shock in the background foam and the transmitted shock in the filament. Following the analysis of [Malamud et al. \(2013\)](#) we can fully describe the post-shock flow behind the incident shock as a function of the incident shock velocity U and the initial state: the densities of the unshocked background and filament (or their contrast ratio δ), their initial pressures, and the adiabatic indexes γ in each material. This planar analysis is suitable for describing the bulk post-shock flow but becomes inaccurate near the axis where radial compression is considerable. U is taken radially away from the initial interface where the shock appears planar (e.g. roughly 200 μm), assumed to be the effective free-streaming limit of the incident shock. In the analysis the CRASH simulations employ both the ideal $\gamma = 5/3$ and the values of γ from equation of state tables created by the PROPACEOS software ([MacFarlane et al. 2006](#)).

In the stationary shock frame, the experimental flow is analogous to the proposed astrophysical case: a dense cylindrical filament flows into the virial boundary of the galaxy under gravitational force, high pressures drive a shock into the filament, the filament collapses, and

along with the dissipative KH instability it disperses its matter into the galactic environment (visualized from the simulation of the experimental system in the right panel of Fig. 2). Fig. 3 idealizes the flow geometry of the stationary incident shock frame, labeled $S1$.

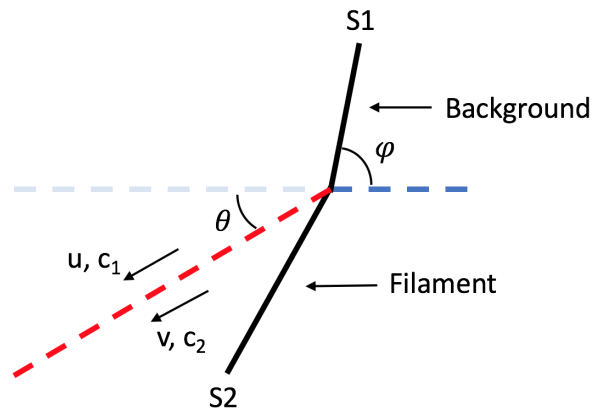


Figure 3. Idealized flow geometry in the stationary shock frame. A background and filament flow into incident shock $S1$ and transmitted shock $S2$, respectively. The dashed line indicates the interface between materials, red denoting the deflected interface.

Transforming to this frame, the Euler balance equations for the case of an oblique shock can be solved to determine the flow field properties. On the key assumption that there is pressure equilibrium on the deflected interface, these equations for planar flows in rectangular

geometry take the form, (Malamud et al. 2013)

$$\rho_0 U \sin \phi = \rho_1 u_1 \sin(\phi - \theta), \quad (1)$$

$$p_0 + \rho_0 U^2 \sin \phi = p_1 + \rho_1 u_1^2 \sin(\phi - \theta), \quad (2)$$

$$\rho_0 \tan \phi = \rho_1 \tan(\phi - \theta), \quad (3)$$

$$\epsilon_0 + \frac{p_0}{\rho_0} + \frac{U}{2} \sin \phi = \epsilon_1 + \frac{p_1}{\rho_1} + \frac{u_1^2}{2} \sin(\phi - \theta). \quad (4)$$

In this frame, the flow with initial density ρ_0 , pressure p_0 , and specific energy ϵ_0 (respective to each material) is seen to enter from right to left through oblique shocks at angles ϕ for the background and $\phi - \theta$ for the filament. Both materials travel with an initial velocity U . Each of the shocked flows then has velocities parallel to the deflected interface (red dashed line), labeled u and v as in Fig. 3, respectively for the shocked background and filament. The velocity difference $\Delta u = |u - v|$ defines the shear velocity at the interface, corresponding to KH evolution. In solving (1)-(4) simultaneously for each material, **where the shocked velocity variable u_1 is u for the background or v for the filament**, a theoretical estimate for the growth rate may be obtained.

2.2. Subsonic, compressible KH evolution on the deflected interface

For the following discussion we assume negligible surface tension and viscosity. For incompressible flow, a perturbation on the interface having a small amplitude to wavelength ratio (i.e. $\lambda \gg h$) will exponentiate at the rate

$$\gamma_{ic} = \frac{k \Delta u}{2} \sqrt{1 - A^2}. \quad (5)$$

where $k = 2\pi/\lambda$ is the wavenumber, $\Delta u = |u - v|$ is the difference in shear speeds in each material parallel to the interface, and $A = (\rho_2 - \rho_1)/(\rho_2 + \rho_1) = (\delta - 1)/(\delta + 1)$ is the Atwood number (Drake 2018). In the so-called linear regime, the perturbation will grow exponentially, according to $h \sim h_0 \exp(\gamma_{ic} t)$; this occurs until approximately $h/\lambda \sim 0.1$.

However, for the compressible case in the limit of $A \rightarrow 0$ the KHI will evolve with a rate

$$\gamma_c = -i \gamma_{ic} \frac{\sqrt{-1 - M_c^2 + \sqrt{1 + 4M_c^2}}}{M_c}, \quad (6)$$

where M_c is defined as the convective Mach number, or $M_c = \Delta u/(c_1 + c_2)$ (Choudhury 1997; Malamud et al. 2013). Here c_1 and c_2 are the sound speeds in the shocked materials. Note in the reference frame of one of the fluids being stationary, a convective Mach of $M_c = 0.5$ corresponds to the transition to supersonic

flow with a Mach number $M = 1$ flow in the moving fluid. **Using the model described in Section 2.1 with an ideal gas with $\gamma = 5/3$, the transition to subsonic Mach flow occurs with an incident shock of 6-7 $\mu\text{m ns}^{-1}$.** This will be employed as the cutoff when seeking a subsonic $M_c < 0.5$ regime later. Additionally Eq. (6) suggests that increasing the shear velocity has the effect of reducing the instability growth rate, stabilizing the KHI; a value of $M_c = \sqrt{2}$ yields an imaginary growth rate, theoretically stifling the instability altogether. Note, that this result was confirmed in full numerical simulations (Malamud et al. 2013).

The KHI evolving on the deflected interface is assumed to evolve in the linear, subsonic, compressible regime, with a growth rate predicted by Eq. (6) and a corresponding timescale $\tau_{KH} = 1/\gamma_c$. However, the initial perturbation wavelength λ is compressed to λ_s , due to the oblique shock compression of the background and filament as discussed in Sec. 2.1. This shocked wavelength is approximated as (Malamud et al. 2013)

$$\lambda_s \approx \lambda \frac{u_c}{U}. \quad (7)$$

The quantity u_c is called the convection velocity, an average speed at which a point on the interface drifts or equivalently, the net velocity at which the KH vortices convect. It can be found by assuming there exists a stagnation point between each pair of KH vortices. At these points, the fluid flow can be approximated as quasi-steady and in pressure equilibrium (Dimotakis 1986). Applying the Bernoulli equation yields

$$\rho_1(u - u_c)^2 = \rho_2(v - u_c)^2. \quad (8)$$

The total time available for KH evolution at any point on the deflected interface is the time it takes that point to travel the length L of the interface, $t_{growth} \approx L/u_c$. Referring to Fig. 3, the deflected interface is assumed to be a straight line, extending from the point of shock continuity between oblique shocks $S1$ and $S2$ to the point where the deflected interface reflects about axis. Thus $L = R_s/\sin \theta$, where R_s is initial radius of the stream.

2.3. Summary of model assumptions and connection to the astrophysical case

Before making the case for hydrodynamic similarity between the experimental and astrophysical systems, here we briefly summarize the model.

- The cold stream of radius R_s in a comoving background system flows through a strong shock whose flow properties in the planar geometry assumption may be described by (1)-(4). The two fluids have infall velocity U and a density contrast δ . In stationary shock frame, the physics of each system will evolve similarly. Similarity will be established in Section 3.1 - 3.2 and the flow solutions discussed in Section 3.3.
- KH on the filament is assumed to evolve exponentially, in the linear growth regime of standard KH formulation. This is justified by the initial wavelength λ , perturbation amplitude h_0 , and compressible KH dynamics quantified by M_c , discussed in Section 3.3
- The dynamics of the system are driven by the ram pressure $P \approx \rho_b U^2$ of the background. The shocked background maintains constant pressure. This has an important consequence in considering radiative cooling, discussed in Section 3.5.
- If the KH growth is prominent, it will have the effect of increasing mixing between the shocked background and filament. The KH could be capable of entraining the entire shocked filamentary region. The conclusions in Section 4 will address this.

3. SCALING

We argue that the physical processes of the laboratory experiment described here and the idealized astrophysical picture are hydrodynamically equivalent on certain length and timescales by establishing scaling relations between the two. Namely, we seek to show the applicability of the Euler equations to the processes, that the same terms in each apply, establish Ryutov scaling between the systems, and address specific scaling of more detailed phenomenon (Ryutov et al. 1999). The first two points follow simply from prior assumptions and assertions, but will be strengthened by global Reynolds, Peclet, collisionality, and similar arguments used to determine physical consistency between the two systems. Ryutov scaling will be established by identifying characteristic state parameters,

$$\tilde{u}_1 \sqrt{\frac{\tilde{\rho}_1}{\tilde{P}_1}} = \tilde{u}_2 \sqrt{\frac{\tilde{\rho}_2}{\tilde{P}_2}}. \quad (9)$$

where subscripts 1 and 2 denote characteristic velocity \tilde{u} , pressure \tilde{P} , and density $\tilde{\rho}$ of each system (Ryutov et al. 1999).

Finally, we make a case for detailed scaling beginning with the idealized system proposed by Mandelker et al. (2016) and Padnos et al. (2018), then addressing the caveats of our system, to include discussions of radiation, geometrical considerations, and gravity.

3.1. Scaling parameter range

The astrophysical scalings can be built from parameter ranges as derived by Mandelker et al. (2016) and Padnos et al. (2018), following the semi-analytical analysis of virial shocks by Dekel and Birnboim (2003) and subsequent work. We again note that in the work of Mandelker et al. (2016) and Padnos et al. (2018), the assumption is that the cold stream is embedded in a stationary, hot galactic background, with *pressure equilibrium* between the stream and background. We begin by assuming the presence of a shock, behind which post-shock pressures exceeds the material pressure of the cold stream, thus driving a shock into and collapsing the filament. For the relevant astrophysical regime, i.e. an unstable galactic regime, we assume the interaction of a cylindrical filament with a planar shock for a galaxy of characteristic mass $M_{12} \sim 10^{12} M_\odot$ around a characteristic redshift of $z \sim 2$. Note that the assumption of a planar shock neglects the spherical geometrical effects. However, this assumption is justified considering the stream radius to virial shock radius ratio, $R_s/R_v \ll 1$. Also assumed is a co-moving background, infalling with the filament that contributes the high pressure post-shock background. Within this picture, no shear occurs between the filament and unshocked background.

The cosmic background plasma can be assumed to be a polytropic hydrogen gas with $\gamma = 5/3$. The virial temperature for a galaxy of this mass and redshift is given by

$$T_v \approx 1.5 \times 10^6 \times M_{12}^{2/3} [3/(1+z)] = 1.5 \times 10^6 K \quad (10)$$

which is taken to be the temperature of the shocked infall (Padnos et al. 2018). The virial shock for such a characteristic galaxy is assumed to remain at the virial radius and the cold stream accretes at a roughly constant infall velocity comparable to the virial velocity $U \sim V_v$. This is estimated from the virial theorem,

$$\frac{3}{5} \frac{GM}{R_v} = \frac{3}{2} \frac{k_B T_v}{m_p} = \frac{1}{2} V_v^2, \quad (11)$$

yielding $U \sim 200 \text{ km s}^{-1}$. This is assumed to be the shock speed.

Since we are not considering an embedded flow, a useful physical scaling parameter here would be the upstream

Parameter	Physical description	Symbol	Cold Stream	Experiment (filament)
Length scale (cm)	Filament radius	R_s	3×10^{21}	0.01
Velocity (cm/s)	(Virial) shock speed	U	2×10^7	3×10^6
Density (gpcc)	Filament density	ρ_s	10^{-26}	1.4
Temperature (eV)	Filament temperature	T_s	86	2
Effective ionization	Average of shocked plasmas	Z	2	10.3
Effective mass number	-	A	1	0.1
Ion Density (cm^{-3})	-	n_i	0.003	1.7×10^{27}

Table 1. Characteristic parameters for the galactic cold stream and experiment as discussed in Section 3.1.

Mach number, defined in stationary shock frame as the speed of the shock over the sound speed in the upstream (unshocked) material $M_b = U/c_s$. Simulations suggest that the streams may have densities $\rho_s = 10^{-26}$ to $10^{-27} \text{ g cm}^{-3}$ and temperatures of $T_s = 10^4 \text{ K}$ and the background material $\rho_b = 10^{-27}$ to $10^{-28} \text{ g cm}^{-3}$. This is further supported by the derived density contrast range of $\delta = 10 - 100$ by Mandelker et al. (2016). For the model here, we assume $\delta = 10$ with $\rho_b = 10^{-27} \text{ g cm}^{-3}$ and $\rho_s = \delta\rho_b$. However, if we consider the unshocked, comoving background material to be on order of stream temperature $T_s = 10^4 \text{ K}$, then the sound speeds on order of 20 km s^{-1} suggest strong accretion shocks at $M_b \sim 10$ for the background. This justifies use of the strong-shock conditions. Note in the radiative analysis of virial shocks, if a shock has receded, it is because the post-shocked material once behind it has cooled, thereby weakening the shock. Further radiation considerations are discussed in Section 3.5.

The radius of the filament is taken as $R_s/R_v \sim 0.005 - 0.05$. Padnos et al. (2018) modifies this estimation to include cosmological inflow but we assume the simplified model presented in Mandelker et al. (2016). From Mandelker et al. (2016) we also take $R_s/\lambda \gtrsim 1$. This constraint on the wavelength λ is perhaps the biggest uncertainty regarding our model assumptions, however, we choose a wavelength that yields experimental time and length scales to ensure a considerable effect of KHI as well as diagnostic capability.

3.2. Applicability of the Euler Equations to describe both systems

We proceed to show that the Euler equations, with negligible heat transport and viscosity, describe these systems in a similar manner.

In the experiment, initial foam and plastic densities are $\rho_b = 0.14 \text{ g cm}^{-3}$ and $\rho_s = 1.4 \text{ g cm}^{-3}$. Thus, laser driven shocks on order of tens of $\mu\text{m ns}^{-1}$ produce highly collisional plasmas, having ion and electron MFP ranging from 10^{-2} to 10^{-6} microns. However at such

sparse densities, the galactic plasma is a little more complex. The fully ionized infall at 10^4 K has ion and electron mean free paths on order of $\lambda_{mfp} \approx 10^{14} - 10^{15} \text{ cm}$, (several thousands of a parsec), and equilibrates on order of 10s of years. With the lowest length scales on order of hundreds of parsecs and millions of years, the collisional mean free path satisfies the condition $\lambda_{mfp} \ll L$, permitting a single fluid description of the dynamics. It is worth noting that collective plasma effects of the magnetized plasma may bring the MFP to 10^{16} cm , and the fluid approximation still holds. Only when the temperature exceeds 10^8 K , and the density drops below $10^{-28} \text{ g cm}^{-3}$ (at the outskirts of a cluster, for example), does the fluid approximation begin to break.

However, at temperatures in excess of 10^4 K radiation emission is strong, and at such low densities the galactic matter is completely unable to entrain the photons and even more so for the post-shocked medium. The mean free paths associated with Compton scattering and Bremsstrahlung are order 10^{26} cm and greater, thus the photons can be considered free-streaming (despite a tremendously high photon viscosity). However, one must address the effect of radiative cooling, to ensure that on relevant time scales cooling effects are minimal. This is considered in Section 3.4.

At present we consider only the adiabatic case, neglecting photon viscosity. For the galactic plasma at 10^6 K assuming a Coulomb logarithm of $\ln \lambda = 24$, the kinematic viscosity is $3 \times 10^{24} \text{ cm}^2 \text{ s}^{-1}$. With length scales on order of the filament radius, roughly $1 \text{ kpc} \sim 3 \times 10^{21} \text{ cm}$ and shock velocities $2 \times 10^7 \text{ cm}^2 \text{ s}^{-1}$, the corresponding Reynolds number is 10^5 .

For the experiment, simulations approximate that the CHI plastic and CH foams reach average ionizations of $Z = 0.1$ at $T = 2 \text{ eV}$ and $Z = 0.9$ at $T = 8 \text{ eV}$, with effective atomic masses $A = 10.3$ and $A = 8.3$, respectively. Taking the Coulomb logarithm to be 1 yields viscosities on order of $1 \text{ cm}^2 \text{ s}^{-1}$ for the foam and 0.04

Parameter	Symbol	Cold Stream	Experiment
Hydrodynamics:			
Localization	l_c/h	1.8×10^{-5}	4.9×10^{-6}
Ryutov number	$\tilde{v} \sqrt{\tilde{\rho}/\tilde{p}}$	2.2	2.3
Heat transport:			
Thermal diffusivity ($\text{cm}^2 \text{s}^{-1}$)	χ	2.4×10^{26}	5.1
Peclet number	Pe	2.5×10^3	6.0×10^3
Momentum transport:			
Thermal viscosity ($\text{cm}^2 \text{s}^{-1}$)	ν	3.2×10^{24}	4.4×10^{-2}
Reynolds number	Re	1.9×10^5	6.8×10^5
Radiation:			
Compton mfp (cm)	l_{rad}	1.3×10^{26}	41
Cooling time	$\tau_{cooling}/\tau$	2.3	-

Table 2. Derived scaling parameters for the galactic cold stream and experiment as described in Section 3.1. While the cooling time of the cold stream is relevant, in the experiment cooling is negligible.

$\text{cm}^2 \text{s}^{-1}$ for the filament, corresponding to Reynolds numbers of roughly 7×10^5 and 3×10^4 , respectively. The characteristic length for both flow descriptions is the filament radius and the characteristic velocity is the shock (infall) speed. Note that these exceed Reynolds numbers required for shear instabilities ($Re \sim 10^3$) and turbulent mixing (Dimotakis 2000). Furthermore, these Reynolds numbers are comparable to those of the adiabatic galactic case, and both systems satisfy that viscous effects are negligible.

Now we wish to ensure that heat transfer is dominated by convection, assessing the thermal conductivity of each system. **For the astrophysical case, the thermal conductivity is $2 \times 10^{26} \text{ cm}^2 \text{s}^{-1}$, yielding a Peclet number of 3×10^3 .** The plastic filament has a conductivity of $0.31 \text{ cm}^2 \text{s}^{-1}$ yielding a Peclet number of roughly 10^5 . The foam being 10 times less dense is roughly 10 times more diffusive, with a Peclet number of 6×10^3 . As such, **the effects of thermal heat transport** can be ignored.

Having determined that these systems are physically consistent, we assess the Ryutov similarity, stated in Table 3.1. Since both systems are shown to be strongly driven, Ryutov similarity is guaranteed. We can choose either post-shock conditions to be characteristic or assume a characteristic pressure that is proportional to the fluid ram pressure $\tilde{p} \sim \tilde{\rho} \tilde{u}^2$ for this purpose. In the next section we assert that the systems are ram pressure dominated. Hydrodynamic evolution then proceeds similarly if both the initial conditions are identical and the shock driver evolves similarly on the timescale $t = L/\tilde{u}$. In future work, we will seek to identify this specific scaling between initial conditions.

3.3. Experimental predictions and projections to the astrophysical case

For the model experiment and the astrophysical analog, the solution of Eqs (1)-(4) for the convective Mach number given in Eq. (6) and other flow properties is shown in Table 3.2. Because both systems are ram pressure dominated, we show that the solutions are fundamentally identical and predict potential KH growth values. We note that the growth time scale is largely geometrical, fixed by the time of travel for a point down the deflected interface (red, dashed line in Fig. 3), and is not sensitive to ΔU for the parameter ranges given here. The KH growth rate, however, is much more sensitive to non-geometrical parameters, quickly stifled by large contrast ratio and high wavelength perturbations $\lambda \sim R_s$, assuming a relatively stable shock velocity of $U \sim 200 \text{ km s}^{-1}$.

The systems with $\gamma_s = \gamma_b = 5/3$ are predicted to be supersonic with a convective Mach of $M_c = 0.87$ and a growth time to KH growth rate ratio $t_{growth}/\tau_{KH} = 3.76$. In the model experiment with $\lambda = R_s = 100 \mu\text{m}$, a $h_0 = 5 \text{ nm}$ perturbation amplitude will grow to $h/\lambda_{shocked} \sim 0.1$ in roughly $0.5 t_{KH}$ cycles. This implies that the growth observed will be out of the linear, exponential growth model after roughly 1.8 ns. With regards to diagnostic capability, for a collapse length estimate of $L = 312 \mu\text{m}$ (neglecting the point of shock reflection) and with a shocked wavelength of $\lambda_s = 77 \mu\text{m}$ we can expect to observe in the linear regime at least the first of roughly four KH unstable peaks on the collapsed interface. At similar shock velocities and for a wavelength greater than this, it is expected that the KH instability will stay longer in the linear regime.

(γ_1, γ_2)	R_s/λ	U [$\mu\text{m ns}^{-1}$]	θ [$^\circ$]	ϕ [$^\circ$]	Δu [$\mu\text{m ns}^{-1}$]	M_c	τ_{KH} [s]	t_{growth}/τ_{KH}
(1.67, 1.67)	1	20	86	19	13.6	0.87	5.41×10^{-9}	3.76
(1.31, 1.92)	1	20	88	21	15.9	1.19	6.75×10^{-9}	3.01
(1.67, 1.67)	1	200	86	19	136	0.87	1.62×10^{14}	3.76
(1.67, 1.67)	3	200	86	19	136	0.87	3.25×10^{14}	11.27

Table 3. Solutions to the oblique shock equations for the idealized flow geometry. Materials with index pairs (γ_1, γ_2) for the background and filament, respectively, with an initial pressure of 10^{10} bar, and flow velocity U produce the listed values of the flow. In order, the first two lines correspond to the experimental model: first, ideal values of γ , then CRASH obtained values (taken from simulation at $t = 80\text{ns}$) using ideal values for lower velocities U , easily obtained with lower laser drives with no significant modifications to the experiment. The following two lines correspond to the astrophysical model.

For example, if $\lambda = 2R_s = 200 \mu\text{m}$, the model predicts that $t_{growth}/\tau_{KH} = 1.88$ so that all four of the deflected peaks will be in the linear regime. However, if $\lambda = 0.5R_s = 50 \mu\text{m}$, then $t_{growth}/\tau_{KH} = 7.52$. **For smaller wavelengths, current radiography diagnostics may become increasingly difficult.** We again note that to be consistent with current astrophysical predictions, $R_s/\lambda \geq 1$.

For the astrophysical case, the same (adiabatic) behavior is expected via hydrodynamic similarity. A consequence of the KH instability is that if KH is allowed enough time to evolve, then significant mixing will occur between the hot shocked background and colder, denser shocked filament. As the KH instability is only able to grow to the effective width of the shocked filament layer (the region between the transmitted shock and the deflected interface as shown in Fig. 3), maximally the shocked layer can be mixed into the background. This does not reduce the unshocked areal mass flux of the filament. However, the KH instability may reduce the areal mass flux of the shocked filament region. The overall effect is inhibited mass delivery towards a critical radius inside the galaxy, where gas may accrete and coalesce into stars. **This** expected behavior is modeled in Fig. 4 where low and high disruption describes the low and high growth time scenarios for a relevant parameter range. We plan to develop this consideration in further work.

3.4. Radiative cooling of the background plasma

Strong radiative cooling in both the shocked background and filament plasmas can significantly alter the collapse dynamics and KH growth. In this section we discuss the radiative cooling model for both plasmas and apply it to the background plasma.

As the photon mean free path, l , is many orders larger than the typical length scale of the system $l \gg L$, the cooling in both plasmas is assumed to be free-streaming with no effect on the optically thin infall. We utilize the

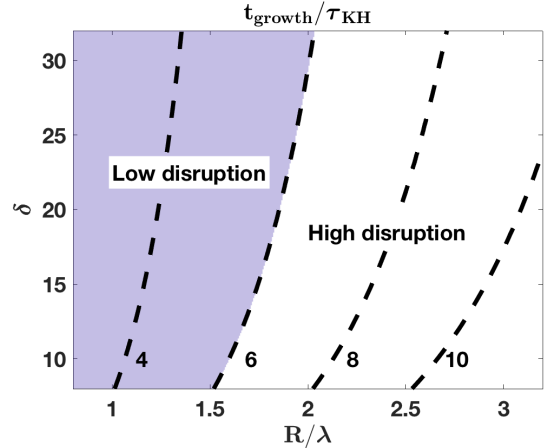


Figure 4. Contours of t_{growth}/τ_{KH} as predicted by the oblique shock model for a range of ratios R_s/λ and δ . As the system becomes dominated by available growth time, the KH becomes more disruptive to the overall collapsed filament evolution, increasing mixing between the shocked background and filament. In order to achieve such enhanced mixing, we estimate several turn over times are required during the stage of KH growth, indicating that t_{growth}/τ_{KH} should exceed $\sim 3 - 5$. Here, we choose $t_{growth}/\tau_{KH} \sim 6$, in order to satisfy the $R_s/\lambda > 1$ condition, discussed in Sec. 3.3.

microscopic cooling function Λ_{mic} as a function of temperature T provided by Sutherland and Dopita (1993); Sutherland et al. (2018), shown in Fig. 5. The microscopic cooling function identifies the power radiated per particle with units $\text{erg cm}^3 \text{s}^{-1}$. Fig. 5 shows two curves of Λ_{mic} for a low density astrophysical plasma in collisional-radiative equilibrium with a hydrogen mass fraction $X = 0.9$, a varying helium mass fraction Y , and a varying mass fraction of elements heavier than helium $Z = 1 - X - Y$ in units of solar metallicity. For both curves, at less than a few eV, hydrogen is molecular and cools inefficiently. At $T \sim 10^4$ K, cooling locally peaks due to Lyman α line emission at roughly $\log \Lambda_{mic} \sim 2 \times 10^{-22} \text{ erg cm}^{-3} \text{ s}^{-1}$. At 10^5 K the second peak appears due to recombination of He. The presence of metallicity $Z > 0$ introduces more atomic bound-

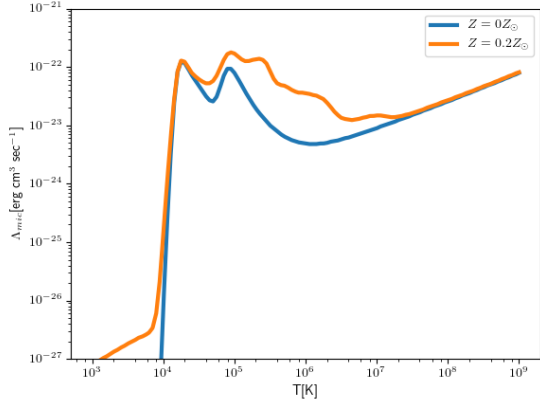


Figure 5. The logarithmic microscopic cooling function, Λ_{mic} , as a function of temperature for a low density astrophysical plasma with a $X = 0.9$ hydrogen mass fraction and varying helium and heavier element mass fractions Y and $Z = 1 - X - Y$, respectively. Based on the MAPPINGS-V plasma code (Sutherland et al. 2018).

bound transitions that increases the cooling rate after being collisionally ionized by free electrons. At much higher than 10^6 K Bremsstrahlung dominates. While the presence of metallicity adds additional features, we assume a $X = 0.9, Y = 0.1$ plasma.

The microscopic cooling function can be used to approximate the cooling time via

$$\tau_{cool} = 4 \times 10^{-36} \frac{A(Z+1)T(eV)}{Z\rho(g\text{ cm}^{-3})\Lambda_{mic}} \quad (12)$$

which is the ratio of the energy density of the plasma to the radiated power per unit volume (Ryutov et al. 1999). For the shocked background at temperatures on order of 10^6 K, the cooling time is $\tau_{cool,b} \approx 2.8 \times 10^{16}$ s. We compare this to the compression timescale of the virial shock

$$\tau_{virial} = \frac{28}{5} \frac{r_s}{|u_0|} (1 - 3\tilde{u}_s)^{-1} \quad (13)$$

suggested by the stability criteria of Dekel and Birnboim (2006). Here r_s is the shock radius (assumed to be the virial radius ($r_s \sim R_v$)), u_0 is the radial velocity of the pre-shock gas (assumed $u_0 = U$), and \tilde{u}_s is a term proportional to the shock velocity. Assuming a stationary shock, i.e. $u_s = 0$, Eq. 13 can be reduced to a simple relation $\tau_{virial} \sim R_v/U$, which is the effective hydrodynamic timescale in the strong-shock limit (less the multiplicative factor of $28/5$). It is a necessary condition for the existence of a virial shock that the cooling timescale of the hot background plasma in the halo is at least on order of this hydrodynamic timescale, **that is that**

$\tau_{cool,b} \gtrsim \tau_{virial}$ **in the background plasma.** For the parameters used here, we note that $\tau_{virial} \approx 8.4 \times 10^{16}$ s. This is on order of the cooling timescale, arguably in the regime in which an accretion shock at the virial radius may exist based on prior order of magnitude estimates.

3.5. Radiative cooling of the filament

For the KH evolution on the filament, the hydrodynamic timescale of interest is the compression time of the filament, the ratio of the filament radius to the sound speed in the filament, $\tau_{hydro} = R_s/c_s \approx 1.1 \times 10^{12}$ s. In the shocked filament the material at a temperature of roughly 10^5 K, the cooling time is $\tau_{cool,s} \approx 2.0 \times 10^{13}$ s. Using an expected astrophysical value of τ_{KH} such as one from the third row of Table 3, the hierarchy of timescales is obtained:

$$\tau_{virial} \sim \tau_{cool,b} > \tau_{KH} > \tau_{cool,s} > \tau_{hydro}. \quad (14)$$

The last equality implies that radiative cooling in the filament is not likely to compress the filament faster than hydrodynamic effects. Thus the assumption that the pressure of the background drives the overall collapse dynamics is reliable. However, because $\tau_{KH} > \tau_{cool,s}$ cooling is likely to be important in describing the KH evolution, as the dynamical rate is $\gamma \sim 1/\tau$. Radiative cooling therefore has the potential to transport energy from the filament to the background faster than KH mixing. We develop this further.

Consider the change in energy density $\rho\epsilon$ of the shocked gases, which is proportional to $\rho T \sim \text{const}$. The denser filament is a much more efficient cooler at roughly 10^5 K than the background at 10^6 K. In removing energy content from the post-shock filamentary gas, radiative cooling removes pressure support behind the oblique shock in the filament. Across the deflected material interface, the post-shock materials have equal pressure $P_0 \approx \rho_b U^2$. The shocked filament material will cool faster than the shocked background, which will maintain its pressure P_0 . The cooling layer then condenses to maintain pressures P_0 at the new cooled temperature T_{cool} . This effectively causes the filament shock to recede, with the velocity of post-shock gas relative to the shock growing increasingly subsonic and thus increasing $p dV$ compression of the post-shock material. Such a reduction in shock-speed has the effect of reducing the post-shock temperature towards 10^4 K, where the cooling rate rapidly drops off. The overall hydrodynamic response is that of a wider deflected angle θ with a shallower post-shock region in the filament at higher density ρ_{cool} . This decreases the sound speed of the material $c_2 \propto \rho^{-0.5}$, increasing the convective Mach M_c .

Alternatively, we may effectively assume the filament is isothermal, having $\gamma = 1$, with a constant cooled temperature of 10^4 K. In this case, the convective Mach number can be estimated as

$$M_c \sim \frac{\Delta u}{\sqrt{P_0} \left(\sqrt{\frac{1}{\rho_b}} + \sqrt{\frac{1}{\rho_{cool}}} \right)}. \quad (15)$$

The Atwood number will increase as the shocked filament goes to higher density, thus reducing the classical KH growth rate. The shear difference between the layers Δu will be smaller, since at higher deflections the velocity component parallel to the interface decreases. An idealized limit thus has $M_c \rightarrow U \sin(\phi - \theta)/c_b$ as $\rho_{cool} \gg \rho_b$, approaching the Mach number of the oblique shock $S1$, $M \sim U/c_b$. Thus, any significant amount of radiative cooling is predicted to stifle the KH instability. To illustrate this effect, the ideal astrophysical model with $R_s/\lambda = 1$ as discussed in Section 3.3 may have a cooled convective Mach of $M_c \sim 1.13$ and $t_{growth}/\tau_{KH} \sim 0.5$ as the shocked filament cools to 10^4 K. **Compared with the value of $M_c = 0.87$ in the third row of Table 3, the effect of cooling may be dramatic.**

Without significant cooling the experimental platform therefore provides the upper adiabatic limit to the astrophysical case, one in which KH may have the most significant role in the hydrodynamic evolution of the filament. If cooling is as significant as the arguments presented above may suggest, then KH might play a very minimal role in the overall dynamics. As we move to more radiative regimes with the experimental platform to study this phenomenon, we will be able to validate more of the physics described.

3.6. Additional instability modes

For the platform and regime discussed we consider conventional surface modes, so that the primary behavior is described by the KH theory presented. These modes grow as a fraction of the virial crossing timescale $t_v \sim R_v/c_b$, where c_b is the sound speed of the background material. However, the series of papers analyzing the instabilities subject to cold filaments, namely (Mandelker et al. 2016; Padnos et al. 2018; Mandelker et al. 2019) identify that body modes may dominate over surface modes for a range of parameters (δ, M_b), where M_b is the background flow Mach number, and geometrical configuration. These grow as instabilities inside the body of the filament, on a time scale of the order of the virial crossing time less the sound crossing time of the stream, $t_v - t_s$, where $t_s \sim 2R_s/c_s$ and c_s is

the sound speed in the filament. For the experimental model, $t_v \sim 100t_s$, suggesting that the virial crossing time dictates the available growth time for both mode types. However, as

$$M_b = M_c \left(1 + \sqrt{1/\delta} \right), \quad (16)$$

with $M_c \sim 0.87$ and $\delta \sim 10$ in our configuration (resulting in stable body modes with $M_c < 1$), we get $M_b \sim 1.15$. This is a little below the critical Mach $M_{crit} = 1.29$, identified in (Mandelker et al. 2016) as

$$M_{crit} = \left(1 + \delta^{-1/3} \right)^{3/2} \quad (17)$$

for which surface modes are expected to dominate.

Padnos et al. (2018) extends this work to the non-linear analysis for 2D slab geometry. However, we note that it is still applicable for cylindrical geometry. Moving to 3D simulations, Mandelker et al. (2019) revealed that the behavior is drastically different for supersonic streams, wherein azimuthal surface modes may grow in a much larger rate than the conventional radial surface modes as expected for 2D streams. For the model experiment, the seeded radial perturbation has $h/\lambda = 0.05$, with no azimuthal modes. However, some azimuthal modes might appear, due to symmetry breaking and **asymmetries introduced in target fabrication**. **The initial amplitude to wavelength ratio of these modes should be very small ($h/\lambda \ll 1$), therefore their amplitude is not expected to exceed that of the radial modes during the experimental timescale.** As we develop this platform further, full 3D calculations will help identify if this is the case for the experiment, as well as provide useful insight into expecting increase in mixing.

3.7. Additional Physics

There are several other physical processes that will need to be considered in future work. These processes are summarized in (Mandelker et al. 2016; Padnos et al. 2018), but briefly they include radiative cooling, the effects of which have been considered in Sec. 3.5; thermal conduction, which is hydrodynamically negligible for large wavelengths as discussed in Sec. 3.2; external gravity of the background on the filament; self gravity of the filament on itself which may lead to filamentary fragmentation, as recently considered in (Aung et al. 2019); magnetic fields that could drastically affect overall KH evolution as well as thermal conduction, as recently considered in (Berlok and Pfrommer 2019); and potentially other effects of galaxy formation. **Some experimental campaigns which include magnetic**

fields for astrophysical relevant Rayleigh-Taylor instability applications are planned for the National Ignition Facility, NIF. Future design work might adapt the current experimental platform to NIF, exploiting both NIF’s much larger laser energy combined with relevant magnetic fields, resulting with a significant magnetic Reynolds number.

4. CONCLUSION

In the present work, a hydrodynamically scaled experiment meant to study the dynamics of filamentary mixing (i.e. KH related mixing) in dark matter halo galaxies is presented. The experimental regime is expected to be close to the adiabatic limit. In this regime, the experimental model presented here may adequately describe the astrophysical case of a KH unstable filament terminating in a virial accretion shock during galaxy formation. Under strong shock scaling the two systems exhibit Ryutov scaling and thus are said to evolve hydrodynamically similarly. Thus the radiography diagnostic used in the experiment may help verify the physics of filament collapse and KH evolution on the deflected interface of the collapsed filament, by enabling the measurement of the angles involved in the flow through oblique shocks as well as the perturbation height during the KH growth. **The experiment will allow the examination of KH growth on a filament interface, and provide insights regarding the largest amount of mixing that might be expected. Radiative cooling effects may be important and would be expected to decrease the mixing.** The

design is based on full, 2D simulations, along with a simple oblique shock model, for estimating expected Mach numbers and growth rates for KH.

In future work, the mixing will be analyzed for its role in reducing aerial mass flux of the shocked filament. As the experiment is expected to be the upper limit as the adiabatic case, this aerial mass flux may be directly translated to a astrophysically relevant aerial mass flux and correspondingly linked to predictions for the star formation rate. Furthermore, the dependency between mixing and instability related quantities such as wavelength and Atwood number will be investigated. We note that future experiments would benefit from the use of larger laser platforms, such as NIF, capable of providing stronger shocks needed to increase radiative cooling rates, along with increasing typical target dimensions for late time evolution.

ACKNOWLEDGEMENTS

This work is funded by the U.S. Department of Energy, through the NNSA-DS and SC-OFES Joint Program in High-Energy-Density Laboratory Plasmas, grant number DE-NA0002956, and the National Laser User Facility Program, grant number DE-NA0002719, and through the Laboratory for Laser Energetics, University of Rochester by the NNSA/OICF under Cooperative Agreement No. DE-NA0001944. YB was supported by ISF grant number 1059/14.

Software: CRASH(vanderHolstet.al.2011), MAPPINGS-V (Sutherland et al. 2018), PROPACEOS (MacFarlane et al. 2006)

REFERENCES

- Han Aung, Nir Mandelker, Daisuke Nagai, Avishai Dekel, and Yuval Birnboim. Kelvin-helmholtz instability in self-gravitating streams. *arXiv preprint arXiv:1903.09666*, 2019.
- I. K. Baldry, K. Glazebrook, J. Brinkmann, Ž. Ivezić, R. H. Lupton, R. C. Nichol, and A. S. Szalay. Quantifying the Bimodal Color-Magnitude Distribution of Galaxies. *Astrophys. J.*, 600:681–694, January 2004.
- Thomas Berlok and Christoph Pfrommer. The impact of magnetic fields on cold streams feeding galaxies. *arXiv preprint arXiv:1904.02167*, 2019.
- Y. Birnboim and A. Dekel. Virial shocks in galactic haloes? *Monthly Notices of the Royal Astronomical Society*, 345(1):349–364, oct 2003.
- Y. Birnboim, Dan Padnos, and Elad Zinger. the Hydrodynamic Stability of Gaseous Cosmic Filaments. *The Astrophysical Journal*, 832(1):L4, 2016.
- N. Bouché, H. Finley, I. Schroetter, M. T. Murphy, P. Richter, R. Bacon, T. Contini, J. Richard, M. Wendt, S. Kamann, B. Epinat, S. Cantalupo, L. A. Straka, J. Schaye, C. L. Martin, C. Péroux, L. Wisotzki, K. Soto, S. Lilly, C. M. Carollo, J. Brinchmann, and W. Kollatschny. Possible Signatures of a Cold-flow Disk from MUSE Using a z? 1 Galaxy-Quasar Pair toward SDSS J1422-0001. *ApJ*, 820(2):121, Apr 2016.
- A. Cattaneo, A. Dekel, J. Devriendt, B. Guiderdoni, and J. Blaizot. Modelling the Galaxy Bimodality: Shutdown above a Critical Halo Mass. *mnras*, 370:1651–1665, August 2006.

- Daniel Ceverino, A. Dekel, and Frederic Bournaud. High-redshift clumpy discs and bulges in cosmological simulations. *Monthly Notices of the Royal Astronomical Society*, 404(4):2151–2169, mar 2010.
- S Roy Choudhury. Nonlinear Evolution of the Kelvin–Helmholtz Instability of Supersonic Tangential Velocity Discontinuities. *Journal of Mathematical Analysis and Applications*, 214:561–586, 1997.
- Nicolas Cornuault, Matthew D. Lehnert, François Boulanger, and Pierre Guillard. Are cosmological gas accretion streams multiphase and turbulent? *Astron. Astrophys.*, 610:A75, March 2018.
- Mark Danovich, A. Dekel, Oliver Hahn, Daniel Ceverino, and Joel Primack. Four phases of angular-momentum buildup in high- z galaxies: from cosmic-web streams through an extended ring to disc and bulge. *Monthly Notices of the Royal Astronomical Society*, 449(2): 2087–2111, may 2015.
- A. Dekel and Y. Birnboim. Galaxy bimodality due to cold flows and shock heating. *Monthly Notices of the Royal Astronomical Society*, 368(1):2–20, 2006.
- A. Dekel, Y. Birnboim, G. Engel, J. Freundlich, T. Goerdt, M. Mumcuoglu, E. Neistein, C. Pichon, R. Teyssier, and E. Zinger. Cold streams in early massive hot haloes as the main mode of galaxy formation. *Nature*, 457(7228): 451–454, 2009.
- Paul E. Dimotakis. Two-dimensional shear-layer entrainment. *AIAA Journal*, 24(11):1791–1796, 1986.
- Paul E. Dimotakis. The mixing transition in turbulent flows. *Journal of Fluid Mechanics*, 409:69–98, 2000.
- R Paul Drake. *High-Energy-Density Physics: Foundation of Inertial Fusion and Experimental Astrophysics*. Springer, 2018.
- Tobias Goerdt and Daniel Ceverino. Inflow velocities of cold flows streaming into massive galaxies at high redshifts. *Monthly Notices of the Royal Astronomical Society*, 450(4):3359–3370, jul 2015.
- BA Hammel, JD Kilkenny, D Munro, BA Remington, HN Kornblum, TS Perry, DW Phillion, and RJ Wallace. X-ray radiographic imaging of hydrodynamic phenomena in radiation-driven materials—shock propagation, material compression, and shear flow. *Physics of plasmas*, 1(5):1662–1668, 1994.
- E. C. Harding, J. F. Hansen, O. A. Hurricane, R. P. Drake, H. F. Robey, C. C. Kuranz, B. A. Remington, M. J. Bono, M. J. Grosskopf, and R. S. Gillespie. Observation of a Kelvin-Helmholtz Instability in a High-Energy-Density Plasma on the Omega Laser. *Physical Review Letters*, 103(4):045005, July 2009.
- O. A. Hurricane, V. A. Smalyuk, K. Raman, O. Schilling, J. F. Hansen, G. Langstaff, D. Martinez, H.-S. Park, B. A. Remington, H. F. Robey, J. A. Greenough, R. Wallace, C. A. Di Stefano, R. P. Drake, D. Marion, C. M. Krauland, and C. C. Kuranz. Validation of a Turbulent Kelvin-Helmholtz Shear Layer Model Using a High-Energy-Density OMEGA Laser Experiment. *Physical Review Letters*, 109(15):155004, October 2012.
- O. A. Hurricane. Design for a high energy density kelvin-helmholtz experiment. *High Energy Density Physics*, 4(3-4):97–102, 2008.
- D. Kereš and L. Hernquist. Seeding the Formation of Cold Gaseous Clouds in Milky Way-Size Halos. *apjl*, 700: L1–L5, July 2009.
- Dušan Kereš, Neal Katz, David H. Weinberg, and Romeel Davé. How do galaxies get their gas? *Monthly Notices of the Royal Astronomical Society*, 363(1):2–28, 2005.
- J.J. MacFarlane, I.E. Golovkin, and P.R. Woodruff. HELIOS-CR – A 1-D radiation-magnetohydrodynamics code with inline atomic kinetics modeling. *Journal of Quantitative Spectroscopy and Radiative Transfer*, 99 (1-3):381–397, may 2006.
- G. Malamud, A. Shimony, W. C. Wan, C. A. Di Stefano, Y. Elbaz, C. C. Kuranz, P. A. Keiter, R. P. Drake, and D. Shvarts. A design of a two-dimensional, supersonic KH experiment on OMEGA-EP. *High Energy Density Physics*, 9(4):672–686, 2013.
- Nir Mandelker, Dan Padnos, A. Dekel, Y. Birnboim, Andreas Burkert, Mark R. Krumholz, and Elad Steinberg. Instability of supersonic cold streams feeding galaxies - I. Linear Kelvin-Helmholtz instability with body modes. *Monthly Notices of the Royal Astronomical Society*, 463(4):3921–3947, 2016.
- Nir Mandelker, Daisuke Nagai, Han Aung, Avishai Dekel, Dan Padnos, and Yuval Birnboim. Instability of supersonic cold streams feeding Galaxies ? III. Kelvin?Helmholtz instability in three dimensions. *Monthly Notices of the Royal Astronomical Society*, 484 (1):1100–1132, 01 2019.
- D Christopher Martin, Donal O’Sullivan, Mateusz Matuszewski, Erika Hamden, Avishai Dekel, Sharon Lapiner, Patrick Morrissey, James D Neill, Sebastiano Cantalupo, Jason Xavier Prochaska, et al. Multi-filament gas inflows fuelling young star-forming galaxies. *Nature Astronomy*, page 1, 2019.
- Dylan Nelson, Mark Vogelsberger, Shy Genel, Debora Sijacki, Dušan Kereš, Volker Springel, and Lars Hernquist. Moving mesh cosmology: tracing cosmological gas accretion. *Monthly Notices of the Royal Astronomical Society*, 429(4):3353–3370, mar 2013.

- Dan Padnos, Nir Mandelker, Y. Birnboim, A. Dekel, Mark R. Krumholz, and Elad Steinberg. Instability of supersonic cold streams feeding galaxies-II. Non-linear evolution of surface and body modes of Kelvin-Helmholtz instability. *Monthly Notices of the Royal Astronomical Society*, 477(3):3293–3328, 2018.
- M. J. Rees and J. P. Ostriker. Cooling, Dynamics and Fragmentation of Massive Gas Clouds - Clues to the Masses and Radii of Galaxies and Clusters. *Mon. Not. R. Astron. Soc.*, 179:541–559, June 1977.
- E. M. Rutter, M. J. Grosskopf, G. Malamud, C. C. Kuranz, E. C. Harding, P. A. Keiter, and R. P. Drake. Comparison between Kelvin-Helmholtz instability experiments on OMEGA and simulation results using the CRASH code. *High Energy Density Physics*, 9:148–151, March 2013.
- D. Ryutov, R. P. Drake, J. Kane, E. Liang, B. A. Remington, and W. M. WoodVasey. Similarity Criteria for the Laboratory Simulation of Supernova Hydrodynamics. *The Astrophysical Journal*, 518(2): 821–832, jun 1999.
- J. Silk. On the Fragmentation of Cosmic Gas Clouds. I - The Formation of Galaxies and the First Generation of Stars. *Astrophys. J.*, 211:638–648, 1977.
- V. A. Smalyuk, O. A. Hurricane, J. F. Hansen, G. Langstaff, D. Martinez, H.-S. Park, K. Raman, B. A. Remington, H. F. Robey, O. Schilling, R. Wallace, Y. Elbaz, A. Shimony, D. Shvarts, C. Di Stefano, R. P. Drake, D. Marion, C. M. Krauland, and C. C. Kuranz. Measurements of turbulent mixing due to Kelvin-Helmholtz instability in high-energy-density plasmas. *High Energy Density Physics*, 9:47–51, March 2013.
- Volker Springel, Simon D.M. White, Adrian Jenkins, Carlos S. Frenk, Naoki Yoshida, Liang Gao, Julio Navarro, Robert Thacker, Darren Croton, John Helly, John A. Peacock, Shaun Cole, Peter Thomas, Hugh Couchman, August Evrard, Jörg Colberg, and Frazer Pearce. Simulations of the formation, evolution and clustering of galaxies and quasars. *Nature*, 435(7042): 629–636, 2005.
- Ralph Sutherland, Mike Dopita, Luc Binette, and Brent Groves. MAPPINGS V: Astrophysical plasma modeling code. *Astrophys. Source Code Libr.*, page ascl:1807.005, July 2018.
- Ralph S. Sutherland and M. A. Dopita. Cooling functions for low-density astrophysical plasmas. *The Astrophysical Journal Supplement Series*, 88:253–327, sep 1993.
- B. van der Holst, G. Tóth, I. V. Sokolov, K. G. Powell, J. P. Holloway, E. S. Myra, Q. Stout, M. L. Adams, J. E. Morel, S. Karni, B. Fryxell, and R. P. Drake. Crash: A block-adaptive-mesh code for radiative shock hydrodynamics - implementation and verification. *The Astrophysical Journal Supplement Series*, 194(2):23, jun 2011.
- S. D. M. White and M. J. Rees. Core condensation in heavy halos: a two-stage theory for galaxy formation and clustering. *Monthly Notices of the Royal Astronomical Society*, 183(3):341–358, jul 1978.
- Y. B. Zel'dovich. Gravitational instability: An approximate theory for large density perturbations. *Astron. Astrophys.*, 500:13, March 1970.